



## Tailoring activated carbons based cocoa pods lignocellulosic materials for Reactive blue 19 adsorption: optimization, adsorption isotherm and kinetic investigation

Anita Zemfack Mekuiko<sup>a</sup>, Donald Raoul Tchui fon Tchui fon<sup>a,b,\*</sup>, Paul Alain Nanssou Kouteu<sup>b,c</sup>, Cyrille Ghislain Fotsop<sup>d</sup>, Christian Sadeu Ngakou<sup>a</sup>, Hermann-Idriss Tiotsop Kuete<sup>a</sup>, Aurelien Bopda<sup>a</sup>, Arnaud Kamdem Tamo<sup>e,f</sup>, Solomon Gabche Anagho<sup>a,\*</sup>

<sup>a</sup>Research Unit of Noxious Chemistry and Environmental Engineering, Department of Chemistry, Faculty of Science, University of Dschang, Dschang, Cameroon, emails: tchui fondonald@yahoo.fr (D.R.T. Tchui fon), sg\_anagho@yahoo.com (S.G. Anagho), mekuikoanita@yahoo.com (A.Z. Mekuiko), cs\_ngakou@yahoo.com (C.S. Ngakou), hermann.kuete@yahoo.fr (H.-I.T. Kuete), aurelienbopda@gmail.com (A. Bopda)

<sup>b</sup>Laboratory of Energy, Materials, Modeling and Method, Department of Process Engineering, National Higher Polytechnic School of Douala, University of Douala, Douala, Cameroon

<sup>c</sup>Process Engineering Laboratory, Ucac-Icam Institute, Cameroon

<sup>d</sup>Institute of Chemistry, Faculty of Process and Systems Engineering, Universität Platz 2, 39106 Magdeburg, Germany, email: fotsopcyril@yahoo.fr (C.G. Fotsop)

<sup>e</sup>Laboratory for Bioinspired Materials BMBT, Institute of Microsystems Engineering IMTEK, University of Freiburg, 79110 Freiburg, Germany

<sup>f</sup>Freiburg Center for Interactive Materials and Bioinspired Technologies FIT, University of Freiburg, 79110 Freiburg, Germany, email: arnaud.kamdem@imtek.uni-freiburg.de (A.K. Tamo)

Received 14 March 2023; Accepted 17 June 2023

### ABSTRACT

The present study reports on the performance of activated carbons derived from cocoa pods impregnated with  $H_3PO_4$  (CCCP) and  $ZnCl_2$  (CCCZn) on the removal of Reactive blue 19 from a simulated wastewater. Central composite design, including three factors namely temperature ( $X_1$ ), concentration of the activating agent ( $X_2$ ) and time ( $X_3$ ) of calcination were used to optimize the production conditions. From the analysis of variance, the most significant variable was the calcination temperature. For CCCP activated carbon, optimum conditions were found as follows:  $X_1$ : 600°C,  $X_2$ : 0.3 M and  $X_3$ : 88 min and for CCCZn, they were 600°C, 0.5 M, and 120 min. The experimental values of iodine number for the both activated carbons were 476.25 and 495.53 mg/g for CCCZn and CCCP, respectively. It was observed that the experimental values obtained were much closer to those predicted by the model. The functional groups on the prepared activated carbons were determined from Fourier-transform infrared spectroscopy and confirmed using Boehm's titration. X-ray diffraction analysis showed the presence of amorphous phases in both activated carbons. The scanning electron microscopy images of both activated carbons showed that the activation stage produced extensive external surfaces with quite irregular cavities and pores. CCCP and CCCZn showed a Brunauer–Emmett–Teller surface area of 435.32 and 430.66 m<sup>2</sup>/g, respectively. Non-linear regression analysis showed that, equilibrium data were best described by the Freundlich model for CCCP and Dubinin–Radushkevich for CCCZn. Kinetic studies showed that the adsorption of Reactive blue 19 was better described by the pseudo-second-order model for CCCP, and the Elovich models CCCZn.

**Keywords:** Cocoa pods; Activated carbon; Response surface methodology; Reactive blue 19 adsorption; Kinetics; Adsorption isotherm

\* Corresponding authors.

## 1. Introduction

Water is considered as a precious and limited resource, which must be managed coherently and rationally. Essential to life and to all economic activities, water is used for domestic, industrial and agricultural purposes. Its discharge into the natural environment in the form of effluents, more or less heavily polluted by heavy metals, hydrocarbons, pesticides and dyes, can have serious consequences in the short or long term on public health and hygiene [1]. As concerns dyes, they are mostly synthetic and today represent a large group of chemical compounds.

World production of synthetic dyes is estimated at 800,000 tonne/y. A portion of these dyes, approximately 140,000 tonne/y, is released into the environment during the manufacturing and dyeing stages of fabrics [2]. Dyes have many applications in different fields, such as dyeing and printing on fibers and fabrics of all kinds, coloring of foodstuffs, as well as colouring of medicines and cosmetics [2]. From a commercial point of view, anthraquinones are the next most important dyes after azo dyes. Due to their high stability, they are widely used in the textile field. Reactive blue 19 belongs to this group of dyes containing the aromatic anthraquinone structure. This family of organic compounds is toxic, carcinogenic, refractory and very resistant to natural biodegradation [3].

Faced with the increasingly marked preponderance of these agro-industrial discharges, much research has been directed towards the establishment of efficient depollution techniques to fix or destroy these pollutants in wastewater. Some of these techniques include reverse osmosis, ion exchange, flocculation, membrane filtration, biodegradation, chemical precipitation and adsorption [4]. These techniques have proven to be effective, but the cost of the equipment required and the difficulty of implementing them considerably limit their application [5]. To overcome these shortcomings, techniques that allow the accumulation of chemical species on the surface of an adsorbent material are increasingly sought.

Activated carbons are carbonaceous adsorbents with a large specific surface area and a well-developed porous structure. They are generally prepared by two methods: by physical activation or by chemical activation. The use of commercial activated carbons remains limited by their high purchase price, their dependence on imported and unavailable raw material such as fossil coal for their production; and this has had major economic consequences [6]. The development of the production of activated carbons from lignocellulosic materials is therefore a promising venture. Large quantities of lignocellulosic materials are generated daily from agricultural and agro-industrial activities as biomass wastes. These wastes are available as an alternative raw material for the production of activated carbons, thereby mitigating the increasing environmental pollution they cause due to their accumulation. These assets have therefore prompted increased research on the production of activated carbons from lignocellulosic materials, which are readily available, abundant and underused. Lignocellulosic materials such as rice waste [7], olives stones and cotton cake [8], sugarcane bagasse [9] have been used for the production of activated carbon.

In this study, cocoa (*Theobroma cacao*) pods were used as raw materials for the production of activated carbons. This choice was motivated by the abundance of this biomass. With a production of between 210,000 and 270,000 tonne/y over the last decade, Cameroon is currently the fifth-largest cocoa producer in the world [10].

The production of a good quality activated carbon requires a perfect mastery of the various stages of the synthesis process and the factors that influence this process. In most of the studies encountered, a factor is set at a certain level while varying the others in order to determine the optimum preparation conditions. This way of proceeding has disadvantages such as: the absence of information on the interactions between the effects of the factors studied, the large number of experiments to be carried out which consequently requires more time and the use of large quantities of reagents and energy [11]. Therefore, the surface response methodology is used to optimize the preparation of activated carbons and better study the influence of different variables during preparation.

Several studies utilizing cocoa pods as an adsorbent to absorb some molecules such as Brilliant green, Rhodamine B, Methyl orange, Malachite green, Malachite blue, Congo red, Methylene blue, Remazol violet, Remazol black, Azur II, Reactive red, Acid violet, Crystal violet, Acid yellow and Acid blue had been done [12–19]. To our knowledge, none of them was used to study the kinetics of the absorption of Reactive blue 19 which is a dye that is reactive, bifunctional, chemically stable, metal-free and highly soluble in water [20].

Hence, the goal of this study was to utilize empty cocoa pods as a lignocellulosic material for the production of highly porous activated carbons by applying response surface methodology (RSM) for the deduce the optimum conditions for the preparation. Furthermore, the kinetic and equilibrium aspects on the adsorption of Reactive blue 19 onto the resulting activated carbons were modeled.

## 2. Materials and methods

### 2.1. Collection and pretreatment of the precursor material

Cocoa pods were used as precursor materials for the production of activated carbons. They were collected as waste residue from the harvesting of cocoa, from Santchou subdivision located in the West Region of Cameroon. The collected cocoa pods were washed thoroughly with distilled water to remove dirt from their surfaces, sun dried and then dried overnight in an oven at 105°C. The dried pods were cut, crushed, ground and then sieved to obtain particles of sizes less than 2 mm.

### 2.2. Chemical activation of the precursor material

The precursor material with particles of diameter less than 2 mm were impregnated with different concentrations of solutions of phosphoric acid and zinc chloride. The mixtures were stirred for 24 h, then filtered and dried at 105°C in an oven. The obtained samples were carbonized in an automatic electric oven (SELECT-HORN) at a temperature ranging between 400°C and 600°C and time from 30 to

120 min. The resulting activated carbons were named according to the activating agents used as follows: CCCP for carbons activated with  $H_3PO_4$  and CCCZn for those activated with  $ZnCl_2$ .

### 2.3. Experimental design

RSM is a collection of mathematical and statistical techniques that are useful for modeling and analyzing problems in which a response of interest is influenced by several variables simultaneously [21]. A standard RSM design called central composite design was applied to investigate the combined effect of several variables and to find the optimum conditions for activated carbon preparation. In this work, the variables used were (i) calcination temperature ( $x_1$ ); (ii) concentration of the activating agent ( $x_2$ ) and (iii) calcination time ( $x_3$ ). The range and levels of these variables are shown in Table 1. The response was the amount of iodine adsorbed ( $Y_1$ ).

A second-degree order polynomial was applied to develop an empirical model which simultaneously correlates the parameters and the targeted response, expressed as follows:

$$Y = b_0 + \sum_{i=1}^n b_{ii}x_i + \left( \sum_{i=1}^n b_{ii}x_i \right)^2 + \sum_{i=1}^{n-1} \sum_{j=i+1}^n b_{ij}x_i x_j \quad (1)$$

where  $Y$  is the predicted response,  $b_0$  is the constant coefficients,  $b_{ii}$  the quadratic coefficients,  $b_{ij}$  the interaction coefficients and  $x_i, x_j$  are the coded values of the variables considered.

The statistical software STATGRAPHICS PLUS VERSION 5.0 was used to analyze the data of the experimental design, analysis of variance (ANOVA) and regression analysis to fit the equations developed.

Using the central composite design, the total number of experiments ( $N$ ) performed were calculated using the relation (2), given as [22].

$$N = 2^n + 2n + n_c = 2^3 + 2(3) + 4 = 18 \quad (2)$$

which consists of  $2^n$  factorial points,  $2n$  axial points, and  $n_c$  central points. The center points were used to determine experimental error and data reproducibility.

### 2.4. Physicochemical characterization

#### 2.4.1. Determination of surface functions by the Boehm method

The acidic surface functional groups such as carboxylics, phenolics and lactonics were determined using the solutions of the three bases NaOH,  $NaHCO_3$  and  $Na_2CO_3$ . In this work, 0.1 g of each activated carbon was introduced into 30 mL of an aqueous solution of 0.1 M concentration of each of these 3 bases. The basic surface functions, were determined by replacing the previous basic solutions with a 0.1 M solution of HCl. The mixtures were stirred by means of an Edmund Bühler GmbH multi-station stirrer for 24 h at room temperature. After filtration, 10 mL of each filtrate was titrated using HCl solution for the acid functions, and the NaOH solution for the basic functions.

Table 1  
High and low levels of variables

Variables	Low value (-1)	Center point (0)	High value (+1)
Carbonization temperature $X_1$ (°C)	400	500	600
Concentration of activating agent $X_2$ (M)	0.3	0.65	1
Carbonization time $X_3$ (min)	30	75	120

#### 2.4.2. Fourier-transform infrared spectrophotometry

The activated carbons were characterized by infrared spectroscopy to identify the functional groups present on their surfaces. The reflection method used in this work is that of attenuated total reflection. The infrared spectra of the activated carbons were recorded using a Nicolet iS5 brand spectrophotometer.

#### 2.4.3. Powder X-ray diffraction

This technique was used to deduce the crystalline or amorphous structure of the activated carbons. For this purpose, 0.1 g of an activated carbon was placed in a cup, an X-rays was directed at it and the diffractogram recorded. The diffraction patterns were recorded using an Empyrean device (PANalytical, Almelo, Netherlands) with a  $Cu \alpha_1$  radiation ( $\lambda = 1.540$ ). The scanning was done between  $0^\circ$  to  $80^\circ$ .

#### 2.4.4. Energy-dispersive X-ray spectroscopy

Energy-dispersive X-ray spectroscopy (EDX) was used to determine the elemental composition of the activated carbons. The elements making up the activated carbon samples were then deduced from the peaks generated by EDX analysis.

#### 2.4.5. Scanning electron microscopy

Scanning electron microscopy (SEM) analysis was used to determine surface morphology of both the activated carbons and raw cocoa pods. It was carried out using SEM analyzer XL30, ESEM, FEI, USA. An electron beam was used to image samples with a resolution down to the nanometer scale. The electrons were emitted from a filament and collimated into a beam in the electron source. The beam was then focused on the sample surface by a set of lenses in the electron column.

#### 2.4.6. Brunauer–Emmett–Teller coupled with Barrett–Joyner–Halenda

The activated carbons prepared had their surface area, pore volume, and maximum pore radius determined using a micrometric sorptometer (Thermo Electron Corporation, Sorptomatic Advanced Data Processing). Prior to analysis, the sample was degassed for 5 h under vacuum at

307.13 K. After degassing, the sample was transferred to the analysis system where it was cooled in liquid nitrogen. The Brunauer–Emmett–Teller (BET) specific surface area of the samples was determined by N<sub>2</sub> adsorption at 77.13 K; cumulative pore volume was calculated using the Barrett–Joyner–Halenda (BJH) model.

2.5. Batch equilibrium experiments and analytical method

A stock solution of Reactive blue 19 of concentration 500 mg/L was prepared. Experimental solutions at desired concentrations were obtained by diluting the stock solution. The different parameters studied were the pH (varied between 2.0–8.0), the contact time (0–150 min), and the initial concentration of Reactive blue 19 (25–80 mg/L). A mass of 0.1 g of activated carbons was brought into contact with 30 mL of experimental solutions. The mixture was stirred at 1500 rpm. At equilibrium, the mixtures were filtered, and the filtrates obtained were analysed using the UV/Vis spectrophotometer at λ<sub>max</sub> value of 418 nm. The amount (Q<sub>ads</sub>) of Reactive blue 19 adsorbed was calculated using the following expression:

$$Q_{ads} = \frac{(C_i - C_e)V}{m} \tag{3}$$

where C<sub>i</sub> and C<sub>e</sub> are the initial and equilibrium concentrations of the Reactive blue 19, and V the volume of its solution, while m is the mass of the activated carbon.

2.6. Modelling theoretical background

In this study, non-linear forms of the two parameter isotherms models and non-linear forms of kinetic models were used. Tables 2 and 3 summarize these models.

3. Results and discussion

3.1. Experimental design

3.1.1. Development of regression model equation

Central composite design was used to develop a correlation between activated carbons preparation variables and the iodine number. The complete experimental design with their responses is presented in Table 4. This table shows that the iodine number of CCCP activated carbons was found to range from 95.17 to 437.80 mg/g, whereas the iodine number of CCCZn activated carbons ranged from 228.42 to 494.91 mg/g. For both types of activated carbons, a higher iodine number was obtained at a temperature of 600°C while the smallest iodine number was obtained at a temperature of 400°C. As a result, the iodine number increases with the increase in calcination temperature. Runs 1–4 at the center point were used to determine the experimental error.

Based on the sequential model sum of squares, the highest order polynomials were used for choosing the model, where the additional terms were significant, and the model was not biased [31]. For both CCCP and CCCZn activated carbons, the quadratic model was selected, as suggested by the software. Eqs. (4) and (5) represent the regression model

for the response, iodine number, in terms of the experimental variables.

$$Y_1(\text{CCCP}) = -1589.11 + 6.62461X_1 - 382.526X_2 + 3.00079X_3 - 0.0051893X_1^2 - 1.01971X_1X_2 + 0.00264389X_1X_3 + 586.384X_2^2 - 0.150952X_2X_3 - 0.0256262X_3^2 \tag{4}$$

$$Y_2(\text{CCCZn}) = -19.7295 - 0.0221402X_1 + 692.762X_2 - 2.73907X_3 + 0.00138221X_1^2 - 0.747786X_1X_2 + 0.000528889X_1X_3 - 275.615X_2^2 + 0.453175X_2X_3 + 0.0162257X_3^2 \tag{5}$$

These models can be used to predict the iodine number for given levels of carbonization temperature (X<sub>1</sub>), activating agent concentration (X<sub>2</sub>) and carbonization time (X<sub>3</sub>). The performance of the model developed was evaluated based on the correlation coefficients R<sup>2</sup>. Depending on the methodology used, a model is validated for a value of correlation coefficient R<sup>2</sup> ≥ 75%. In this work, this value was 88% for CCCP and 83% for CCCZn, indicating there is a good agreement between experimental data and the predicted data [32]. This result indicates that 88% and 83% of

Table 2 Non-linear forms of two-parameters isotherm models

Isotherms	Non-linear forms	References
Langmuir	$Q_e = \frac{Q_m K C_e}{1 + K C_e}$	[23]
Freundlich	$Q_e = K_f C_e^{1/n}$	[24]
Dubinin–Radushkevich	$Q_e = Q_m \exp(-K \epsilon^2)$ $\epsilon = RT \ln \left( 1 + \frac{1}{C_e} \right)$	[25]
Temkin	$Q_e = Q_m \frac{RT}{\Delta Q} \ln(AC_e)$	[26]

Table 3 Non-linear forms of kinetic models

Kinetics	Non-linear forms	References
Pseudo-first-order	$q_t = q_e (1 - e^{-k_t t})$	[27]
Pseudo-second-order	$q_t = \frac{k_2 q_e^2 t}{1 + k_2 q_e t}$	[28]
Elovich	$q_t = \frac{\ln(\alpha\beta)}{\beta} + \frac{\ln t}{\beta}$	[29]
Intraparticle diffusion	$q_t = k_{id} t^{1/2} + C$	[30]

Table 4  
Experimental design matrix for optimization using central composite design

Run order	Activated carbons preparation parameters			Responses			
	$X_1$	$X_2$	$X_3$	$H_3PO_4$		$ZnCl_2$	
				IN $Y_1$ (mg/g)	Pre. value	IN $Y_2$ (mg/g)	Pre. value
1	500(0)	0.65(0)	75(0)	228.42	266.26	399.73	430.48
2	500(0)	0.65(0)	75(0)	209.38	219.55	323.59	333.33
3	500(0)	0.65(0)	75(0)	304.56	266.26	342.63	333.33
4	500(0)	0.65(0)	75(0)	342.63	387.58	323.59	333.33
5	500(0)	0.65(0)	30(-1)	152.28	143.42	304.56	354.77
6	400(-1)	0.65(0)	75(0)	114.21	117.29	247.45	255.79
7	500(0)	0.30(-1)	75(0)	342.63	266.26	228.42	301.47
8	500(0)	1.00(1)	75(0)	323.59	288.60	342.63	297.66
9	400(-1)	1.00(1)	30(-1)	133.24	120.57	247.45	262.97
10	400(-1)	0.30(-1)	30(-1)	152.28	197.23	266.49	228.71
11	600(1)	1.00(1)	75(0)	209.38	266.26	399.73	333.33
12	600(1)	0.65(0)	120(1)	304.56	311.44	418.77	438.52
13	400(-1)	1.00(1)	120(1)	95.17	126.28	285.52	295.33
14	600(1)	1.00(1)	120(1)	266.49	272.85	399.73	377.61
15	400(-1)	0.30(-1)	120(1)	171.31	158.64	228.42	232.52
16	500(0)	0.65(0)	120(1)	266.49	231.50	399.73	388.60
17	600(1)	0.30(-1)	30(-1)	418.77	385.16	475.87	459.03
18	600(1)	0.30(-1)	120(1)	437.80	447.97	494.91	472.36

$X_1$ : Carbonization temperature ( $^{\circ}C$ ),  $X_2$ : Activating agent concentration (M),  $X_3$ : Carbonization time (min).  
 $Y_1$  and  $Y_2$ : iodine number (IN), Exp. value: Experimental value, Pre. value: Predicted value.

the variation of iodine number of the CCCP and CCCZn can be explained by the proposed models.

### 3.1.2. Analysis of variance

A positive value of a coefficient in Eqs. (4) and (5) reveals a positive effect on iodine number while a negative value of a coefficient reveals a negative effect on iodine number. In this regard, one can say that carbonization temperature, carbonization time, interaction between carbonization temperature and carbonization time and quadratic effect of activating agent concentration influence positively the iodine number of CCCP while the other coefficients influence it negatively. As for CCCZn, carbonization temperature, carbonization time, interaction between carbonization temperature and activating agent concentration and quadratic effect of activating agent concentration influence the iodine number negatively, while the other coefficients influence it positively. To evaluate the significance of these effects, the ANOVA of the quadratic models was done and are listed in Tables 5 and 6. Values of probability ( $P$ -value) less than 0.05 indicate that the model terms are significant while  $P$ -values greater than 0.05 indicate that the model terms are not significant [33]. In this study, the factors  $X_1$  and  $X_2$  were significant for the iodine number of CCCP while  $X_1$  was significant for the iodine number of CCCZn as indicated by the higher  $F$ -ratios and  $P$ -value less than 0.05 [34].

### 3.1.3. Response surface, Pareto diagram and main effects of factors on iodine number

The results obtained are presented by Fig. 1.

Fig. 1 shows the response surfaces, the Pareto diagram and the influence of the various parameters during the preparation of activated carbons. For this plot, calcination time was fixed at zero level ( $t = 75$  min). As can be seen from this figure, the iodine number generally increases with increase in temperature. The Pareto diagram shows that temperature was the most significant factor, while calcination time and concentration of the two activating agents did not show much effect on the iodine number. This was expected, because as the calcination time increases, the more the structure of the raw material becomes porous, which causes compression on the walls of the various pores and consequently decreases their volume. Deng et al. [35] had also found that calcination time did not show much effect on the surface area obtained for activated carbons prepared from apricot stones.

### 3.1.4. Validation of the experimental model

Optimization of the activation parameters was done using STATGRAPHICS Plus version 5.0 software. The results are shown in Table 7. The optimal activated carbons were obtained using the following preparation conditions: 600 $^{\circ}C$  calcination temperature, 0.3 M phosphoric acid and 88 min

calcination time for CCCP sample, as well as 600°C calcination temperature, 0.5 M zinc chloride and 120 min calcination time for CCCZn sample. As for the iodine number, the optimal values were 473.21 and 488.42 mg/g for CCCP and CCCZn, respectively. It was observed that the experimental values obtained were in good agreement with the values predicted by the model, with relatively small errors between the predicted and the experimental values.

Table 5  
Analysis of variance using iodine number for CCCP

Source	Sum of squares	Df	Mean square	F-ratio	P-value
$X_1$	94,243.30	1	94,243.30	35.47	0.0003*
$X_2$	24,494.60	1	24,494.60	9.22	0.0162*
$X_3$	2,934.71	1	2,934.71	1.10	0.3240
$X_1^2$	7,296.84	1	7,296.84	2.75	0.1361
$X_1X_2$	10,190.20	1	1,019.20	3.83	0.0859
$X_1X_3$	1,132.40	1	1,132.40	0.43	0.5322
$X_2^2$	13,981.5	1	13,981.5	5.26	0.0510
$X_2X_3$	45.22	1	45.22	0.02	0.8994
$X_3^2$	7,296.84	1	7,296.84	2.75	0.1361

$R^2 = 88\%$

Df: Degree of freedom

Table 6  
Analysis of variance for iodine number (CCCZn)

Source	Sum of squares	Df	Mean square	F-ratio	P-value
$X_1$	83,481.10	1	83,481.10	34.86	0.0004*
$X_2$	36.29	1	36.29	0.02	0.9051
$X_3$	1,304.39	1	1,304.39	0.54	0.4816
$X_1^2$	517.688	1	517.69	0.22	0.6543
$X_1X_2$	5,480.00	1	5,480.00	2.29	0.1688
$X_1X_3$	45.3152	1	45.32	0.02	0.8940
$X_2^2$	3,088.84	1	3,088.84	1.29	0.2889
$X_2X_3$	407.55	1	407.55	0.17	0.6908
$X_3^2$	2,925.35	1	2,925.35	1.22	0.3012

$R^2 = 83\%$

Table 7  
Model validation

	$X_1$ (°C)	$X_2$ (mol/L)	$X_3$ (min)	Y (mg/g)		Error (%)
				Obs. value	Fit. value	
CCCP	600	0.3	88	495.53	473.21	4.50
CCCZn	600	0.5	120	476.25	488.42	2.49

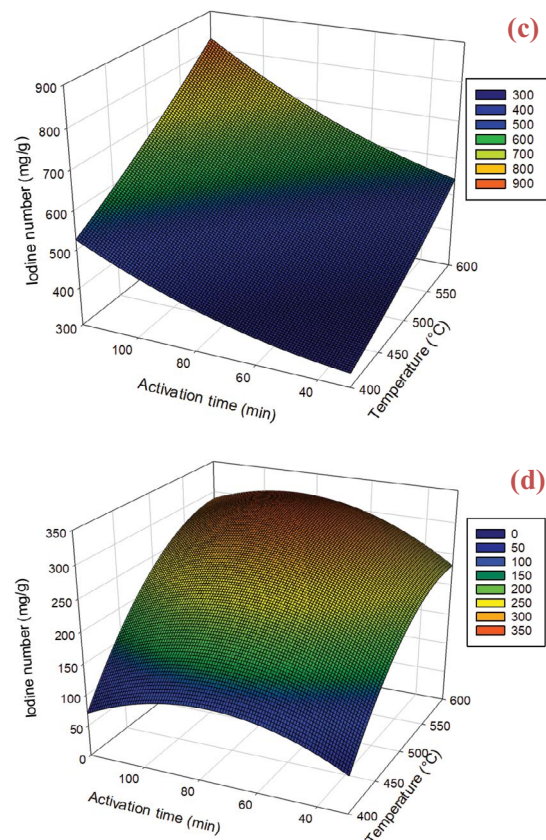
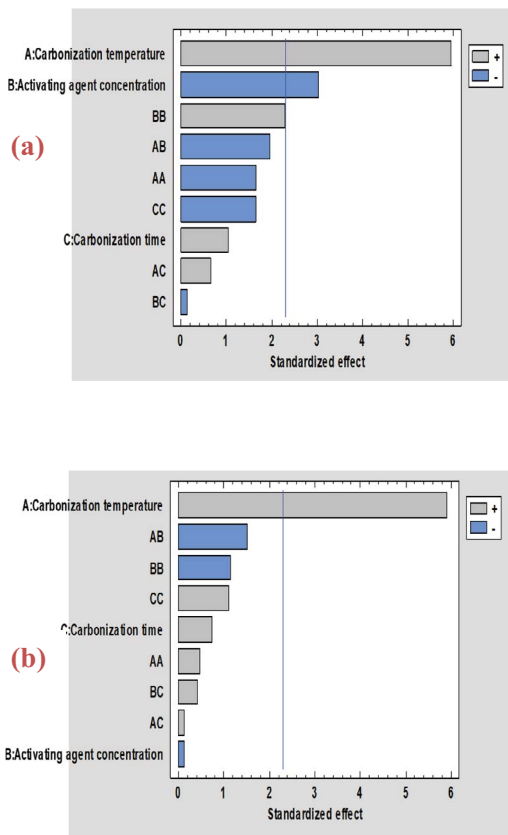


Fig. 1. Three-dimensional response surfaces, Pareto diagrams: CCCZn (a), CCCP (b) and effects of factors investigated: CCCZn (c), CCCP (d).

### 3.2. Fourier-transform infrared analysis of activated carbons

From the Fourier-transform infrared (FTIR) analysis it was possible to identify the different functional groups present on the surface of the activated carbons. The infrared spectra obtained for the biomass and the activated carbons are illustrated by Fig. 2.

The results obtained show that the functional groups were not the same in the raw material and activated carbons. Some of the functional groups in CCC such as the O–H stretching vibrations have disappeared. This result can be explained by the fact that the high temperature in the activation process broke down some intermolecular bonds, leading to the disappearance of some functional groups which were originally present in the raw material. These include:

- 3,291.17  $\text{cm}^{-1}$ ; O–H stretching vibrations;
- 2,925.12  $\text{cm}^{-1}$ ; C–H asymmetric stretching;
- Around 1,650  $\text{cm}^{-1}$ ; C=O stretching in esters;
- 1,028.82  $\text{cm}^{-1}$ ; C–O stretching vibrations in carboxylic acids, alcohols, phenols and esters.

The spectra of activated carbons CCCZn and CCCP have the same shape, which means that they have the same chemical functions on their surfaces. Two peaks are observed on these spectra:

- Peak around 1,600  $\text{cm}^{-1}$ ; C=C stretching aromatic;
- Peak between 1,250 and 1,000  $\text{cm}^{-1}$ ; C–O stretching vibrations in carboxylic acids, alcohols, phenols and esters.

With regards to these spectra, cocoa pods exhibit hydroxyl functional groups, including hydrogen bonding (3,600–3,200  $\text{cm}^{-1}$ ), which is much less prevalent in both activated carbons. The reduction of hydrogen bonding shows that the phosphoric acid and zinc chloride act as a dehydrating agents reacting with the raw materials [8].

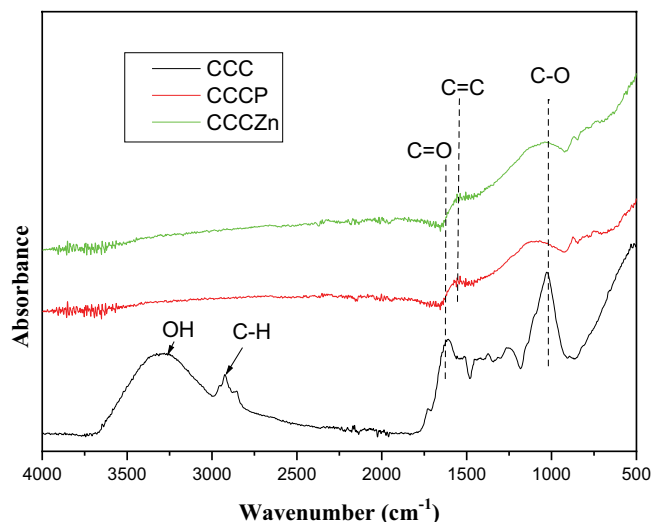


Fig. 2. Fourier-transform infrared spectra of cocoa pods and the activated carbons CCCP and CCCZn.

### 3.3. Energy-dispersive X-ray spectroscopy

Fig. 3a shows the EDX elemental microanalysis and the EDX mapping of the raw material. It can be seen from these that the raw cocoa pods consist only of carbon and oxygen. The absence of hydrogen is attributed to the EDX analytical technique which cannot highlight atoms with a number of protons lower than 4.

Fig. 3b presents the EDX analysis (a-1 and b-1) and elemental mapping (a-2 to a-5, and b-2 to b-5) for the activated carbons obtained from the cocoa pods biomass; where the a-series refer to CCCP and the b-series refers to CCCZn, carbon and oxygen are the main elements found in both activated carbons, with carbon having the highest percentage: 86.7% in CCCZn and 86.9% in CCCP. This result shows that the carbonized materials, with the high percentage of carbon, close to 90% clearly shows that these materials are indeed activated carbons. The presence of oxygen detected in the EDX spectra of the activated carbons certainly comes from the numerous surface oxygenated functions. Moreover, the presence in trace amounts of the elements P and Zn is due to the residues from the activating agents  $\text{ZnCl}_2$  and  $\text{H}_3\text{PO}_4$ . These results are in agreement with those obtained from FTIR and the surface functions, which lead to the conclusion that oxygen is the predominant heteroatom in the activated carbons.

With regard to the EDX analysis, the two activated carbons reveal traces of phosphorus (1.2%) and zinc (1.8%). On the contrary, when looked at from the point of view of the mapping analyses, there is an unequal distribution of these two compounds in the activated carbons. Showing that their percentages vary according to the method chosen for analysis. This inequality can also affect the adsorbent properties of these two materials because it could lead to a repulsion of the pollutant molecules, depending on their nature.

### 3.4. Boehm's titration results

The surface functionality analysis of activated carbon was also done by Boehm titration. The results of Table 8 show that, the quantity of acidic groups is higher than the basic groups on the surface of both activated carbons. The presence of basic and acidic sites on the surfaces of these activated carbons gives them a double effectiveness for the acidic or basic chemical nature of the pollutant to be treated. These results are in agreement with those obtained from FTIR and EDX spectroscopies which highlight the presence of oxygenated groups on the surface of the activated carbons.

### 3.5. SEM analysis

The SEM analysis was used to determine the morphology of both the activated carbons and the raw cocoa pods. SEM micrographs of CCCP, CCCZn and raw cocoa pods are shown in Fig. 4.

The SEM images of CCCP and CCCZn show that the activation stage produced extensive external surfaces with quite irregular cavities and pores. These pores result from the evaporation of the chemical activating reagents ( $\text{H}_3\text{PO}_4$  and  $\text{ZnCl}_2$ ) during carbonization, thereby leaving empty spaces [36]. The SEM image of the raw cocoa powder shows that its surface presents few cavities or voids. This microporosity

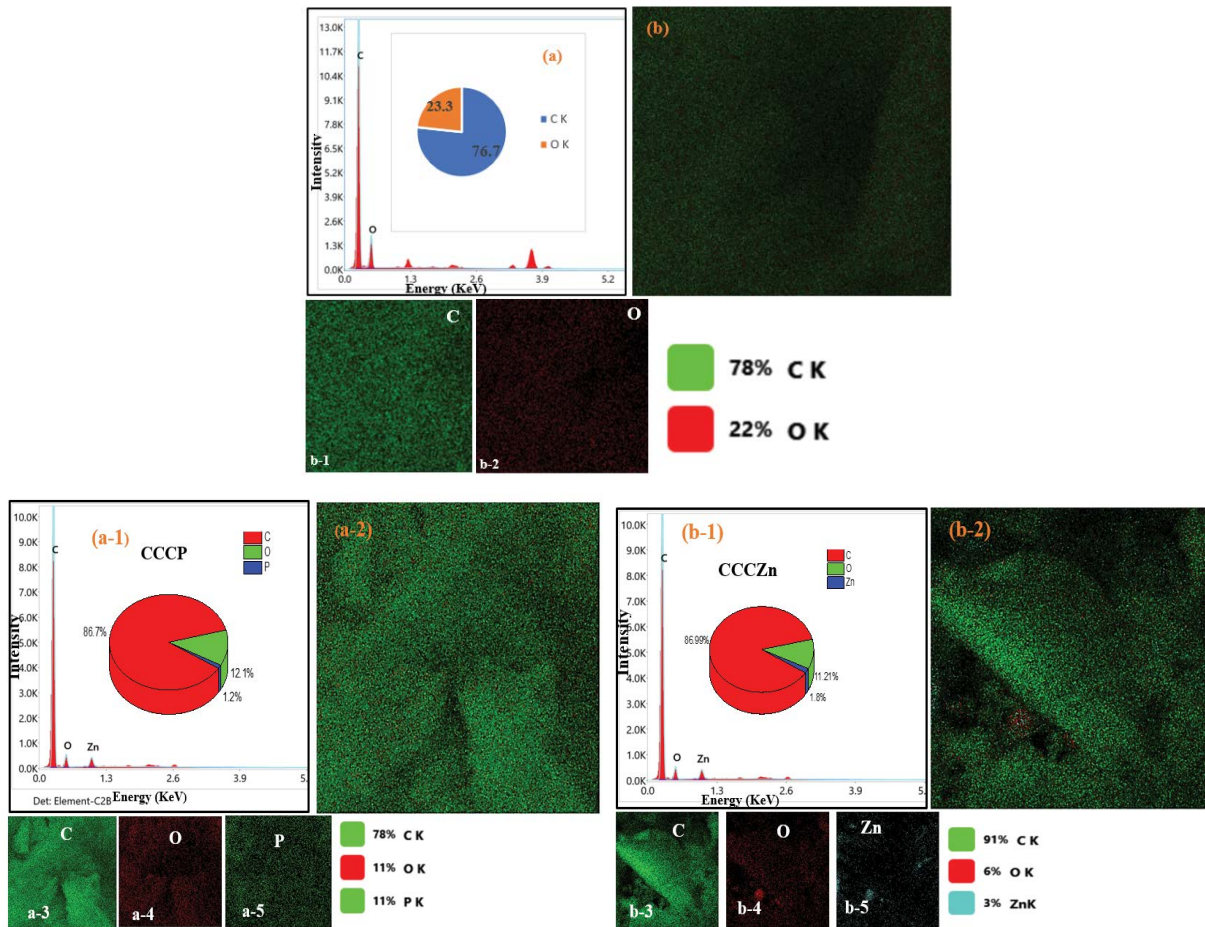


Fig. 3. (a) EDX elemental compositions (a), EDX-mapping (b) and element distribution mapping of C and O (from b-1 to b-2, respectively) for the cocoa pods. (b) EDX elemental compositions (a-1) and (b-1), mapping analysis (a-2) and (b-2) and elemental distribution mapping (from a-3 to a-5) and (from b-3 to b-5) of CCCP and CCCZn, respectively.

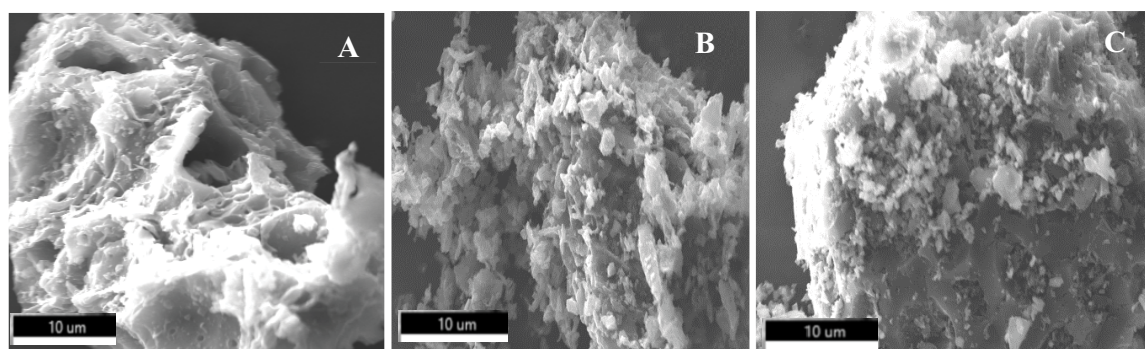


Fig. 4. SEM images of the raw cocoa powder (A) and the activated carbon samples (B) CCCP and (C) CCCZn.

observed by the SEM results in the raw material can also be explained by the fact that cocoa pods contain a much higher content of cellulose and low content of lignin [37].

### 3.6. X-ray diffraction analysis of powdered activated carbons

The X-ray diffraction (XRD) of the activated carbons CCCP and CCCZn are shown in Fig. 5. In these figures,

there is a complete absence of sharp peaks in the spectrum of CCCP. This reveals that activated carbon CCCP prepared from cocoa pods using phosphoric acid has mainly an amorphous structure [38]. On the other hand, the diffraction patterns of CCCZn shows many peaks: an intense peak at  $2\theta = 37^\circ$  and several other short peaks at  $2\theta = 31^\circ, 34^\circ, 48^\circ, 56^\circ, 62^\circ, 67^\circ$ , attributable to the crystalline phases of the metal. This means that there is an increasing regularity of

the crystalline structure, which will result in a better alignment of the layer.

Furthermore, the crystallinity index (CrI) was calculated using Eq. (6), to evaluate the impact of activation agent.

$$\text{CrI} = \frac{\text{Area of all the crystalline peaks}}{\text{Area of all the crystalline and amorphous peaks}} \times 100 \quad (6)$$

The crystallinity index values of the both activated carbons calculated using Origin Pro 2019 software are 60.00% and 8.34% for CCCZn and CCCP, respectively. These results thus validate the crystalline nature of the activated carbon (CCCZn) obtained by using zinc salt as an activating agent and the status of amorphous carbon (CCCP) for that obtained from phosphoric acid. These result are similar to those reported by Mafo et al. [34].

### 3.7. BET/BJH analysis

The specific surface area and the pore structure of the activated carbons were characterized by nitrogen adsorption

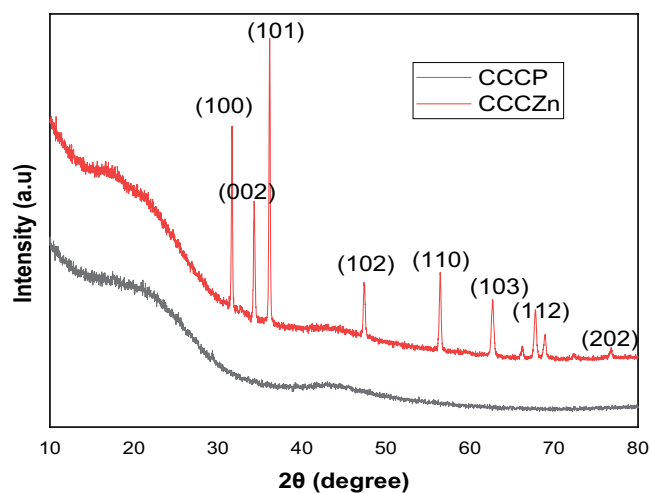


Fig. 5. Powdered X-ray diffraction of CCCP and CCCZn.

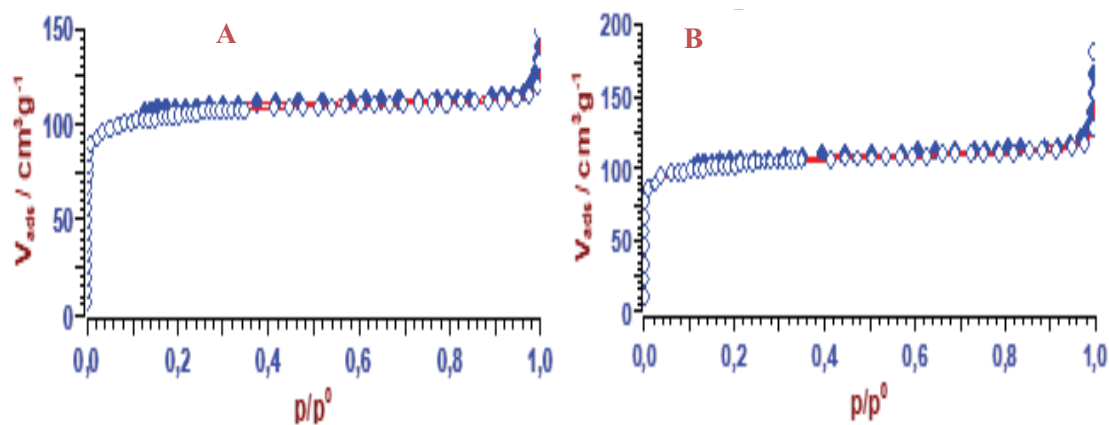


Fig. 6. Adsorption–desorption curves of nitrogen at 77.13 K for CCCP (A) and CCCZn (B).

at 77 K. Fig. 6 shows typical  $N_2$  adsorption–desorption isotherms of CCCP and CCCZn activated carbons. According to IUPAC classification, both isotherms are a mixture of type I and type IV. From Fig. 6, significant adsorption was observed from about  $P/P_0 = 0.4$  with an  $H_4$  type hysteresis loop, reflecting the simultaneous presence of micropores and mesopores [39]. This observation was confirmed with the structural properties presented in Table 9.

### 3.8. Adsorption study

#### 3.8.1. Adsorption kinetics modelling

The kinetic models used to describe the adsorption of Reactive blue 19 are the pseudo-first-order, pseudo-second-order, Elovich, and intraparticle models. The plots of the kinetic models are presented in Fig. 7A and B for both activated carbons. The corresponding constants are summarized in Table 10.

The results in Table 10 show that the coefficients of determination of pseudo-first-order, pseudo-second-order and Elovich models are close to unity. These linear models show that there is competition between chemical and physical interactions during the adsorption of the Reactive blue 19. Based on the low values of  $\chi^2$ , the pseudo-second-order and Elovich models better describe the adsorption of Reactive blue 19 onto CCCP and CCCZn, respectively. This was confirmed by the low values of their RSME and HYBRID error functions. Other researchers like

Table 8  
Total acid and basic groups on surface of activated carbons

	Activated carbons	
	CCCP	CCCZn
Carboxylic (meq/g)	0.36	0.36
Lactonic (meq/g)	0.06	0.15
Phenolic (meq/g)	0.36	0.33
Total acid (meq/g)	0.78	0.84
Total basic (meq/g)	0.09	0.15
Character	Acid	Acid

Zainal et al. [19] found the pseudo-second-order model as the best fit for the adsorption of a dye onto activated carbon made from cocoa pods and activated with  $ZnCl_2$ . The kinetic model of pseudo-second-order highlights interactions of a chemical nature between the adsorbate and the adsorbent [40]. It reveals that the rate of sorption of Reactive blue 19 onto CCCP depends on the available active sites on the activated carbon and the concentration of the Reactive blue 19 in the aqueous phase [16]. The adsorption is monolayer and it can be said that chemisorption dominates the adsorption process of Reactive blue 19 onto CCCP activated carbon. The Elovich model assumes that the surface of CCCZn activated carbon is heterogeneous [41].

### 3.8.2. Adsorption isotherm modeling onto CCCP and CCCZn

In this study, equilibrium data were fitted onto four two-parameter isotherms: Langmuir, Freundlich, Temkin and Dubinin–Radushkevich. The plots of the isotherm models are presented in Fig. 8A and B for both samples. The corresponding constants are summarized in Table 11.

The results in Table 11 show that all the models can be used to describe the adsorption of Reactive blue 19 onto the two activated carbons, CCCP and CCCZn. This is justified by their high values of the coefficient of determination  $R^2$ . The maximum monolayer coverage of Reactive blue 19 onto the different activated carbons elaborated with the Langmuir model (18.134 and 10.388 mg/g for CCCP and CCCZn, respectively) is higher than that obtained by De Luna et al. [42]; who activated cocoa pods with sulfuric acid for the removal of diclofenac in aqueous solution, and they

obtained a value of 0.47411 mg/g. Although all the models have high  $R^2$  values, the low values of  $\chi^2$  and those of the error functions RSME and HYBRID show that the best models that describe the adsorption isotherms of Reactive blue 19 are those of Freundlich for CCCP and Dubinin–Radushkevich for CCCZn. A similar result was obtained by Bello et al. [14] for the adsorption of Remazol violet onto an activated carbon made from cocoa pod.

The results from the Freundlich isotherm model suggest that the adsorption process occurs on heterogeneous surfaces, with a non-uniform distribution of the heat of adsorption over this surface, thereby showing multilayer adsorption [43]. The value of the Freundlich constant  $n$  is greater than 1, indicating that the adsorption is favorable.

The positive values of the adsorption energies obtained from the Temkin model means that the adsorption process is exothermic. The low values of the adsorption energy obtained by the Dubinin–Radushkevich model ranging between 8 and 16 kJ/mol, suggest that ion exchange is the dominant process [43].

### 3.8.3. Mechanism

There are many active sites involved in the adsorption phenomena on the surface of activated carbons. These active sites come from the raw material used and the fabrication process of activated carbon. Surface active sites are mainly oxygenated sites: carboxyl, hydroxyl, quinone, carbonyl, lactone groups; and optionally amino sites [44]. Regarding CCCP and CCCZn, information provided by the FTIR analysis and Boehm titration, supplemented by EDX/

Table 9  
Parameters of the porous structure of CCCP and CCCZn

	$S_{BET}$ ( $m^2/g$ )	Micropore			Mesopore		
		$S_{BET}$ ( $m^2/g$ )	Cumulative pore volume ( $cm^3/g$ )	Maximum pore radius (nm)	$S_{BET}$ ( $m^2/g$ )	Cumulative pore volume ( $cm^3/g$ )	Maximum pore radius (nm)
CCCP	505.46	495.64	0.1662	0.2856	9.82	0.0131	1.296
CCCZn	483.19	468.97	0.1638	0.2701	14.22	0.0217	1.6822

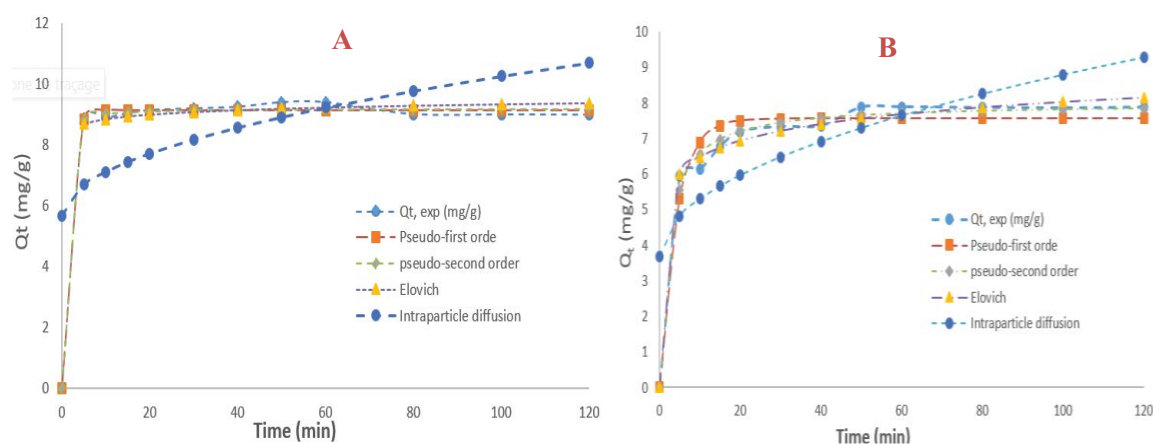


Fig. 7. Plots of non-linear kinetic models for activated carbons CCCP (A) and CCCZn (B).

Table 10  
Non-linear parameters of kinetic models for adsorption of Reactive blue 19 onto CCCP and CCCZn

N°	Model	Constant	Value	R <sup>2</sup>	χ <sup>2</sup>	RSME	HYBRID
CCCP							
1.	Pseudo-first-order	Q <sub>e</sub> (mg/g)	9.134	0.999	0.030	0.158	0.025
		K <sub>1</sub> (min <sup>-1</sup> )	0.690				
2.	Pseudo-second-order	Q <sub>e</sub> (mg/g)	9.198	0.999	0.002	0.147	0.021
		K <sub>2</sub> (g/min·mg)	0.528				
3.	Elovich	α (mg/g·min)	735	0.999	0.005	0.217	0.047
		β (g/mg)	4.568				
4.	Intraparticle diffusion	K <sub>p</sub> (mg/g·min <sup>0.5</sup> )	0.459	0.977	0.512	2.160	4.659
		C (mg/g)	5.658				
CCCZn							
1.	Pseudo-first-order	Q <sub>e</sub> (mg/g)	7.566	0.996	0.253	0.426	0.226
		K <sub>1</sub> (min <sup>-1</sup> )	0.242				
2.	Pseudo-second-order	Q <sub>e</sub> (mg/g)	7.987	0.999	0.006	0.218	0.059
		K <sub>2</sub> (g/min·mg)	0.057				
3.	Elovich	α (mg/g·min)	965.139	0.999	0.005	0.201	0.050
		β (g/mg)	1.476				
4.	Intraparticle diffusion	K <sub>p</sub> (mg/g·min <sup>0.5</sup> )	0.512	0.989	0.282	1.434	2.567
		C (mg/g)	3.680				

Table 11  
Non-linear parameters of isotherm models for adsorption of Reactive blue 19 onto CCCP and CCCZn

N°	Model	Constant	Value	R <sup>2</sup>	χ <sup>2</sup>	RSME	HYBRID
CCCP							
1.	Langmuir	Q <sub>max</sub> (mg/g)	18.134	0.991	0.070	0.808	1.005
		K <sub>L</sub> (L/mg)	0.035				
2.	Freundlich	K <sub>F</sub> (L/mg)	1.602	0.993	0.055	0.715	0.786
		N	1.967				
3.	Temkin	a (L/mg)	0.308	0.992	0.063	0.767	0.906
		b (J/mol)	595.236				
4.	Dubinin–Radushkevich	Q <sub>max</sub> (mg/g)	14.364	0.991	0.074	0.832	1.066
		K (L/mg)	0.003				
		E (kJ/mol)	12.909				
CCCZn							
1.	Langmuir	Q <sub>max</sub> (mg/g)	10.388	0.995	0.027	0.433	0.389
		K <sub>L</sub> (L/mg)	0.076				
2.	Freundlich	K <sub>F</sub> (L/mg)	1.998	0.989	0.068	0.688	0.980
		N	2.755				
3.	Temkin	a (L/mg)	0.656	0.994	0.033	0.480	0.478
		b (J/mol)	1039.463				
4.	Dubinin–Radushkevich	Q <sub>max</sub> (mg/g)	9.423	0.996	0.020	0.377	0.295
		K (L/mg)	0.002				
		E (kJ/mol)	15.811				

SEM showed that their surfaces present both acidic and basic functions. These chemical functions constitute nucleophilic and electrophilic sites capable of reacting with the

quinone and amine groups and the six electrons of the benzene nucleus of Reactive blue 19. Fig. 9 shows possible interactions contributing to the mechanism of Reactive blue 19

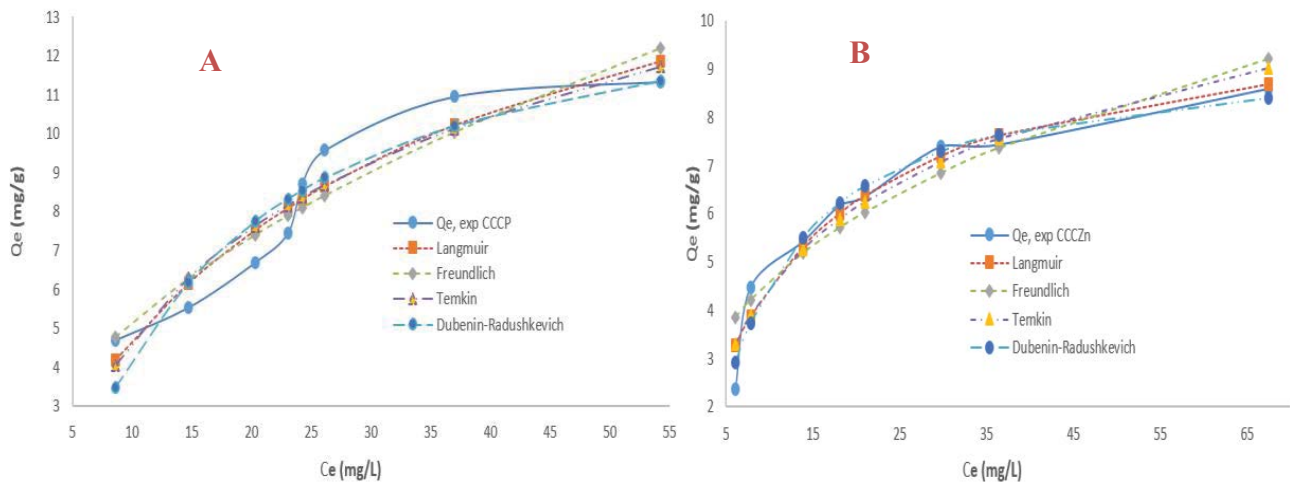


Fig. 8. Non-linear isotherms plot of CCCP (A) and CCCZn (B) activated carbons.

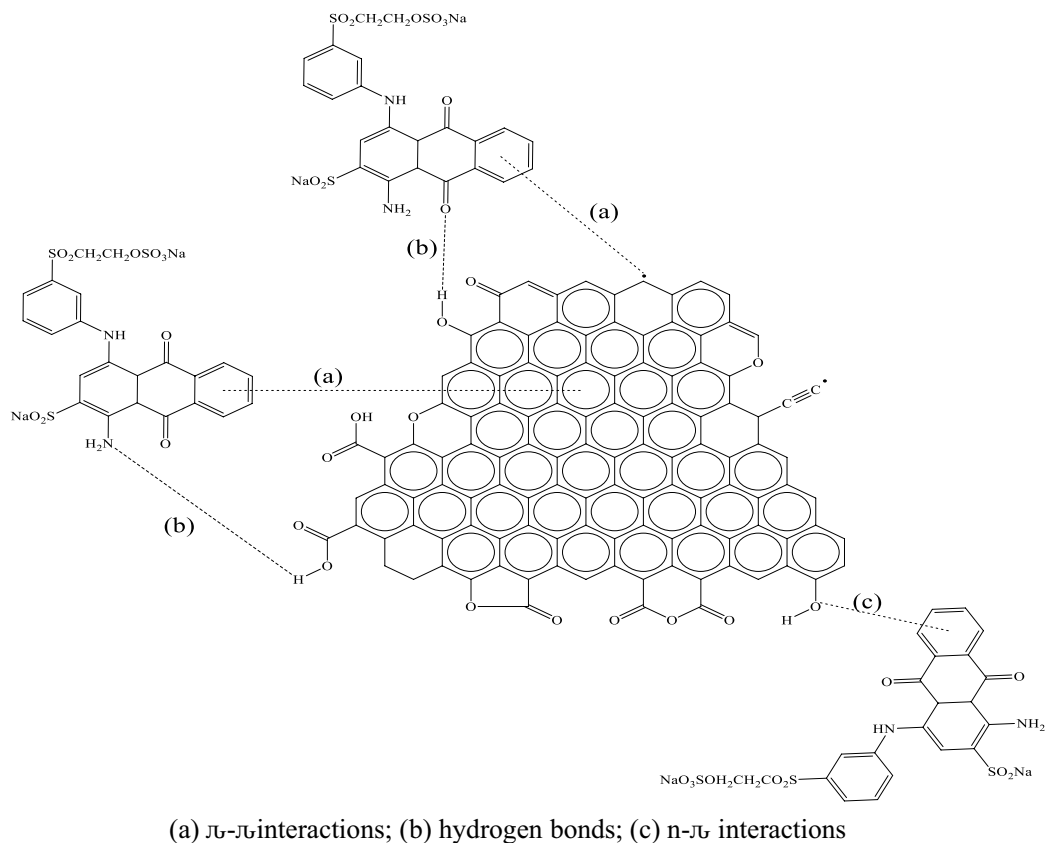


Fig. 9. Possible interactions contributing to the mechanism of Reactive blue 19 adsorption on CCCP and CCCZn.

adsorption on CCCP and CCCZn, knowing that they have the same surface functions.

Kinetic studies show that there is competition between chemical and physical interactions during the adsorption, the main physical mechanisms involved are based on the Van der Waals forces and hydrogen bonds. Balarak et al. [45] made similar observations during their work on adsorption of Acid blue 92 dye from aqueous solutions by single-walled carbon nanotubes [45]. On the other hand,

$n$ - $\pi$  and  $\pi$ - $\pi$  interactions are observed between the aromatic nucleus of activated carbon or with unpaired electrons located at the edge of the sheets of activated carbon.

#### 4. Conclusion

This work was aimed at preparing two activated carbons based on cocoa pods by chemical activation. A central composite design was conducted to study the effects

of three activated carbon preparation parameters, which were the calcination temperature, the calcination time and the concentration of activating agents, on the iodine number. Quadratic models were developed to correlate the preparation variables to the response; the experimental values were observed to be close to the predicted values. The optimal activated carbons were obtained using 600°C calcination temperature, 0.3 M concentration of  $H_3PO_4$  and 88 min calcination time for CCCP resulting in 495.53 mg/g of iodine number. For CCCZn, the optimal conditions were 600°C, 0.5 M, 120 min resulting in 476.25 mg/g of iodine number. Various functional groups on the prepared activated carbons were determined from FTIR which was confirmed by using Boehm's titration and EDX analysis. XRD analysis showed that CCCP activated carbons are amorphous while CCCZn activated carbons have a crystalline structure compared to the crystalline phases of the metal. The SEM images of both activated carbons showed that the activation stage produced extensive external surfaces with quite irregular cavities and pores. CCCP activated carbon showed a BET surface area of 435.32 and 430.66  $m^2/g$  for CCCZn. The kinetic models used to describe the adsorption of Reactive blue 19 were the pseudo-first-order, pseudo-second-order, Elovich, and intraparticle models. Kinetic studies showed that the pseudo-second-order and Elovich models better describe the adsorption of Reactive blue 19 onto CCCP and CCCZn, respectively. Equilibrium data were fitted by four two-parameter isotherms. The best models used to describe the adsorption isotherm of Reactive blue 19 are those of Freundlich and Dubinin-Radushkevich for the activated carbons CCCP and CCCZn, respectively.

### Conflicts of interest

The authors declare that there are no conflicts of interest.

### Acknowledgements

We appreciate the technical assistance of the Researchers of Material and Process Engineering Team (MPET)/RU-NOCHEE of the Department of Chemistry, University of Dschang, Cameroon. The authors also appreciate the support of Mafo Mokue Sandrale and Ngongang Nesta with whom we discussed and had a good time during the manipulation and all their help during this stage. The authors also thank the assistance of Mr. FOUA OTTOU from CICAM.

### References

- [1] A.P. Vieira, S.A. Santana, C.B. Bezerra, H.S. Silva, J.P. Chaves, J.P. de-Melo, F. da Silva, C. Airolti, Kinetics and thermodynamics of textile dye adsorption from aqueous solutions using babassu coconut mesocarp, *J. Hazard. Mater.*, 166 (2009) 1272–1278.
- [2] H.B. Mansour, O. Boughzala, D. Dridi, D. Barillier, L. Chekir-Ghedira, R. Mosrati, Les colorants textiles sources de contamination de l'eau: criblage de la toxicité et des méthodes de traitement, *Rev. Sci. Eau.*, 24 (2011) 209–238.
- [3] M. Laabd, A. El Jaouhari, H. Chafai, A. Nouh, M. Bzzaoui, O.A. Albourine, Etude cinétique et thermodynamique de l'adsorption des colorants monoazoïques sur la polyaniline, *J. Environ. Sci.*, 6 (2015) 1049–1059.
- [4] A.M.S. Ngueabou, R.F.T. Tagne, D.R.T. Tchuiwon, C.G. Fotsop, A.K. Tamo, S.G. Anagho, Strategy for optimizing the synthesis and characterization of activated carbons obtained by chemical activation of coffee husk, *Mater. Adv.*, 3 (2022) 8361–8374.
- [5] C.M. Ncibi, B. Mahjoub, M. Seffen, Etude du processus de biosorption du chrome(VI) par une biomasse méditerranéenne: *Posidonia oceanica* (L) delile, *J. Water Sci.*, 21 (2008) 441–449.
- [6] G. McKay, G. Ramprasad, P.P. Mowli, Equilibrium studies for the adsorption of dyestuffs from aqueous solutions by low-cost materials, *Water Air Soil Pollut.*, 29 (1986) 273–283.
- [7] T.D.R. Tchuiwon, S.G. Anagho, J.M. Ketcha, G.N. Ndifor-Angwafor, J.N. Ndi, Kinetics and equilibrium studies of adsorption of phenol in aqueous solution onto activated carbon prepared from rice and coffee husks, *Int. J. Eng. Technol. Res.*, 2 (2014) 166–173.
- [8] A. Bopda, D.R.T. Tchuiwon, G.N. Ndifor-Angwafor, G. Doungmo, S.G. Anagho, Non-linear equilibrium and kinetic study of the adsorption of 2,4-dinitrophenol from aqueous solution using activated carbon derived from a olives stones and cotton cake, *Afr. J. Environ. Sci. Technol.*, 13 (2019) 366–379.
- [9] M. Valix, W.H. Cheung, G. McKay, Preparation of activated carbon using low temperature carbonization and physical activation of high ash raw bagasse for acid dye adsorption, *Chemosphere*, 56 (2004) 493–501.
- [10] G. Lescuyer, L. Boutinot, P. Goglio, S. Bassanaga, Analyse de la chaîne de valeur cacao au Cameroun, Value chain analysis for development, 2020 (VCA4D CTR 2016/375–804).
- [11] M.A. Bezerra, R.E. Santelli, E.P. Oliveira, L.S. Villar, L.A. Escalera, Response surface methodology (RSM) as a tool for optimization in analytical chemistry, *Talanta*, 76 (2008) 965–977.
- [12] A.O. Araoye, O.S. Agboola, O.S. Bello, Insights into chemically modified cocoa pods for enhanced removal of an anti-malaria drug, *Chem. Data Collect.*, 36 (2021) 100775, doi: 10.1016/j.cdc.2021.100775.
- [13] O.S. Bello, M.A. Ahmad, Adsorptive removal of a synthetic textile dye using cocoa pod husks, *Toxicol. Environ. Chem.*, 93 (2011) 1298–1308.
- [14] O.S. Bello, T.T. Siang, M.A. Ahmad, Adsorption of Remazol Brilliant Violet-5R reactive dye from aqueous solution by cocoa pod husk-based activated carbon: kinetic, equilibrium and thermodynamic studies, *Asia-Pac. J. Chem. Eng.*, 7 (2012) 378–388.
- [15] B.M. Córdova, J.P.S. Cruz, T.V.O. Huamani-Palomino, R.G. Baena-Moncada, A.M. Baena-Moncada, Simultaneous adsorption of a ternary mixture of Brilliant green, Rhodamine B and Methyl orange as artificial wastewater onto biochar from cocoa pod husk waste. Quantification of dyes using the derivative spectrophotometry method, *New J. Chem.*, 44 (2020) 8303–8316.
- [16] O.A.A. Eletta, A.G. Adeniyi, J.O. Ighalo, D.V. Onifade, F.O. Ayandele, Valorisation of Cocoa (*Theobroma cacao*) pod husk as precursors for the production of adsorbents for water treatment, *Environ. Technol. Rev.*, 9 (2020) 20–36.
- [17] Pua, F. Ling, M.S. Sajab, C.H. Chia, S. Zakaria, I.A. Rahman, M.S. Salit, Alkaline-treated cocoa pod husk as adsorbent for removing methylene blue from aqueous solutions, *J. Environ. Chem. Eng.*, 1 (2013) 460–465.
- [18] G. Rodríguez-Arellano, J. Barajas-Fernández, R. García-Alamilla, L.M. Lagunes-Gálvez, A.H. Lara-Rivera, P. García-Alamilla, Evaluation of cocoa beans shell powder as a bioadsorbent of Congo red dye aqueous solutions, *Materials*, 14 (2021) 2763, doi: 10.3390/ma14112763.
- [19] N.A. Zainal, S. Ibrahim, B. Arifin, Preparation and application of zinc chloride-modified cocoa (*Theobroma cacao*) pod husk-based carbon for the removal of acid dyes, *Mater. Sci. Forum*, 889 (2017) 221–225.
- [20] É.V. Nascimento, A.M. Garrido Pedrosa, M.J.B. Souza, Development of  $La_xCa_{1-x}MnO_3$  materials for Bezaktiv blue

- removal in aqueous media, *Water Sci. Technol.*, 83 (2021) 2793–2808.
- [21] D.C. Montgomery, *Design and Analysis of Experiments*, 5th ed., John Wiley and Sons, New York, USA, 2001.
- [22] R. Azargohar, A.K. Dalai, Production of activated carbon from *Luscar char*: experimental and modeling studies, *Microporous Mesoporous Mater.*, 85 (2005) 219–225.
- [23] A.L. Djoumbissie, D.R.T. Tchuiwon, C.D. Atemkeng, I.H.T. Kuete, G. Doungmo, A.C.D. Tayo, S.G. Anagho, J. Ngoune, Kinetic and isotherm studies of the adsorption phenacetin onto two copper porous coordination compounds: non-linear regression analysis, *J. Chem.*, 2022 (2022) 2828860, doi: 10.1155/2022/2828860.
- [24] A.O. Dada, A.P. Olalekan, A.M. Olatunya, O. Dada, Langmuir, Temkin and Dubinin–Radushkevich isotherms studies of equilibrium sorption of Zn<sup>2+</sup> unto phosphoric acid modified rice husk, *IOSR J. Appl. Chem.*, 3 (2012) 38–45.
- [25] M.I. Temkin, V. Pyzhev, Kinetics of ammonia synthesis on promoted iron catalyst, *Acta Phys. Chim.*, 12 (1940) 327–356.
- [26] S. Lagergren, About the theory of so-called absorption of soluble substances, *Kungliga Svenska Vetenskapsakademiens Handlingar*, 24 (1898) 1–39.
- [27] Y.S. Ho, G. McKay, Pseudo-second-order model for sorption process, *Process Biochem.*, 34 (1999) 451–465.
- [28] S.H. Chien, W.R. Clayton, Application of Elovich equation to the kinetics of phosphate release and sorption in soils, *Soil Sci. Soc. Am. J.*, 44 (1980) 265–268.
- [29] W.J. Weber, J.C. Morris, Kinetic of adsorption of carbon from solution, *J. Sanit. Eng. Div.*, 89 (1963) 31–59.
- [30] M.A. Jamaluddin, K. Ismail, M.A. Mohd Ishak, Z. Ab Ghani, M. Abdullah, M.T. Safian, S.S. Idris, S. Tahiruddin, M.F. Yunus, N.I.N. Mohd Hakimi, Microwave-assisted pyrolysis of palm kernel shell: optimization using response surface methodology (RSM), *Renewable Energy*, 55 (2013) 357–365.
- [31] S. Sugashini, K.M.S. Begum, Optimization using central composite design (CCD) for the biosorption of Cr(IV) ions by cross linked chitosan carbonized rice husk (CCACR), *Clean Technol. Environ. Policy*, 15 (2013) 293–302.
- [32] J. Goupy, L. Creighton, *Introduction aux plans d'expériences*, 3e édition, Dunod, Paris, 2001, 336P.
- [33] J.N. Sahu, J. Achatya, B.C. Meikap, Optimization of production conditions for activated carbons from tamarind wood by zinc chloride using response surface methodology, *Bioresour. Technol.*, 10 (2010) 1974–1982.
- [34] S.G. Mafo, D.R. Tchuiwon, C.S. Ngakou, C.G. Fotsop, P.A. Koufeu, G. Doungmo, G.N. Ndifor Angwafor, S.G. Anagho, Study of the degradation of Bezaktiv Brilliant Blue by the Fenton process using a prepared ferromagnetic activated carbon from rubber seed hull as heterogeneous catalyst, *Desal. Water Treat.*, 287 (2023) 200–213.
- [35] H. Deng, G. Zhang, X. Xu, G. Tao, J. Dai, Optimization of preparation of activated carbon from cotton stalk by microwave assisted phosphoric acid chemical activation, *J. Hazard. Mater.*, 182 (2010) 217–224.
- [36] A. Bopda, S.G.M. Mafo, J.N. Ndongmo, G.T. Kenda, C.G. Fotsop, I.-H.T. Kuete, C.S. Ngakou, D.R.T. Tchuiwon, A.K. Tamo, G.N. Ndifor Angwafor, S.G. Anagho, Ferromagnetic biochar prepared from hydrothermally modified calcined mango seeds for Fenton-like degradation of indigo carmine, *C-J. Carbon Res.*, 8 (2022) 81, doi: 10.3390/c8040081.
- [37] A. Omri, M. Benzina, Characterization of activated carbon prepared from a new raw lignocellulosic material: *Ziziphus spina-christi* seeds, *Tunisia J. Chem. Soc.*, 14 (2012) 175–183.
- [38] Y. Sun, Q. Yue, B. Gao, L. Huang, X. Xu, Q. Li, Comparative study on characterization and adsorption properties of activated carbons with H<sub>3</sub>PO<sub>4</sub> and H<sub>4</sub>P<sub>2</sub>O<sub>7</sub> activation employing *Cyperus alternifolius* as precursor, *Chem. Eng. J.*, 181–182 (2012) 790–797.
- [39] Y.S. Ho, Review of second-order models for adsorption systems, *J. Hazard. Mater.*, B, 136 (2006) 681–689.
- [40] T.E. Khalif, H. Altaher, A.R. Reda, Adsorptive removal of Cu(II) ions by date pits: kinetic and equilibrium studies, *Environ. Eng. Manage. J.*, 15 (2016) 2719–2732.
- [41] I.H.T. Kuete, R.D.T. Tchuiwon, A. Bopda, C.S. Ngakou, G.N.A. Nche, S.G. Anagho, Adsorption of indigo carmine onto chemically activated carbons derived from the Cameroonian agricultural waste garcinia cola nut shells and desorption studies, *J. Chem.*, 2022 (2022) 1–19.
- [42] M.D.G. De Luna, W. Murniati, Budianta, K.K.P. Rivera, R.O. Arazo, Removal of sodium diclofenac from aqueous solution by adsorbents derived from cocoa pod husks, *J. Environ. Chem. Eng.*, 5 (2017) 1465–1474.
- [43] N.V.O. Sousa, V.C. Tecia, S.B. Honorato, C.L. Gomes, F.C.F. Baros, S.M.A. Araujo, P.T.C. Freire, R.F. Nascimento, Coconut bagasse treated by thiourea ammonia solution for cadmium removal: kinetics and adsorption equilibrium, *Biochem. Res.*, 7 (2012) 1504–1524.
- [44] S.D.B. Maazou, H.I. Hima, M. Mousbahou, Elimination du chrome par du charbon actif élaboré et caractérisé à partir de la coque du noyau de balanites aegyptiaca, *Int. J. Biol. Chem. Sci.*, 11 (2017) 3050–3065.
- [45] D. Balarak, N.M. Zafariyan, C.A. Igwegbe, K.K. Onyechi, J.O. Ighalo, Adsorption of Acid blue 92 dye from aqueous solutions by single-walled carbon nanotubes: isothermal, kinetic, and thermodynamic studies, *Environ. Processes*, 8 (2021) 869–888.